# Electronic Supplementary Information

## Ni loaded on N-doped carbon encapsulated tungsten oxide nanowires as an alkaline-stable electrocatalyst for water reduction

Cuncai Lv,[a] Guoying Yan,[a] Xiaobo Wang,[a] Linjie Gao,[a] Shichen Xu,[b] Xingyuan San,[a] Shufang Wang*[a], Yaguang Li*[a], Zhipeng Huang*[b]

[a]Key Laboratory of High-precision Computation and Application of Quantum Field Theory of Hebei Province, Hebei Key Lab of Optic-electronic Information and Materials, The College of Physics Science and Technology, Hebei University, Baoding 071002, P. R. China. E-mail: sfwang@hbu.edu.cn, yaguang_1987@126.com.

[b]School of Chemical Science and Engineering, Institute for Advanced Study, Tongji University, Shanghai, 200092, P. R. China. E-mail: zphuang@tongji.edu.cn.

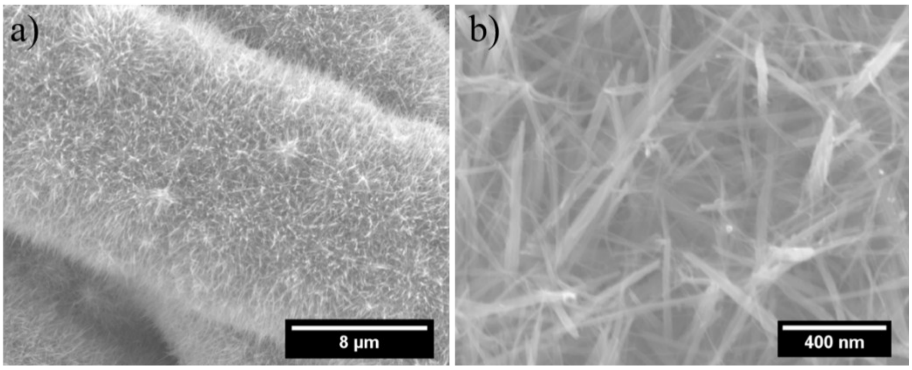


**Figure S1.** (a) Low- and (b) high-magnification SEM images of $WO_x$ precursor loaded on CFP.

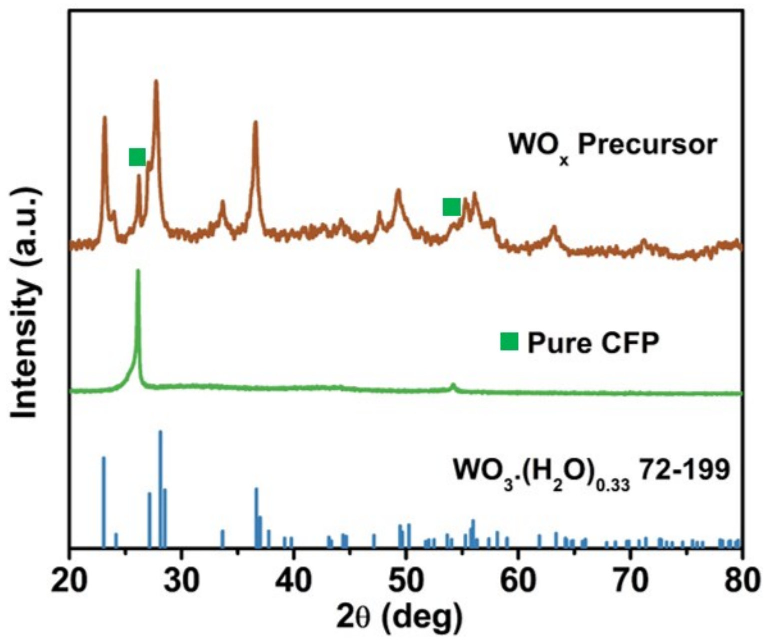


**Figure S2.** XRD pattern of $WO_x$ precursor. The peaks of CFP are marked by blue square.

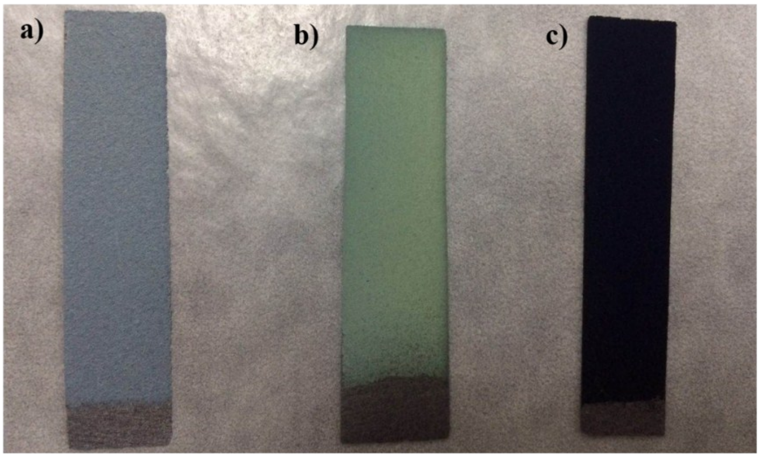


**$WO_x$ precursor** **$WO_x$** **$O_v$-$WO_x$@NC**

**Figure S3.** Optical photograph of the (a) $WO_x$ precursor, (b) $WO_x$, (c) $O_v$-$WO_x$@NC.

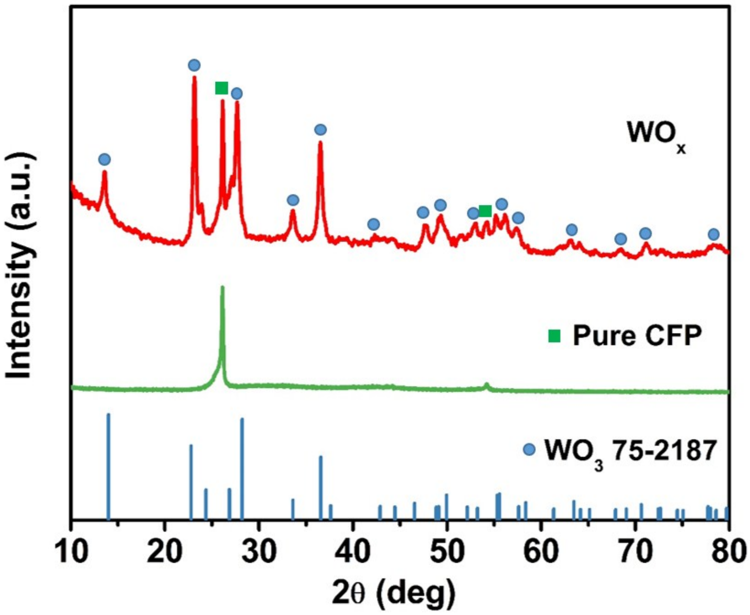


**Figure S4.** XRD pattern of $WO_x$.

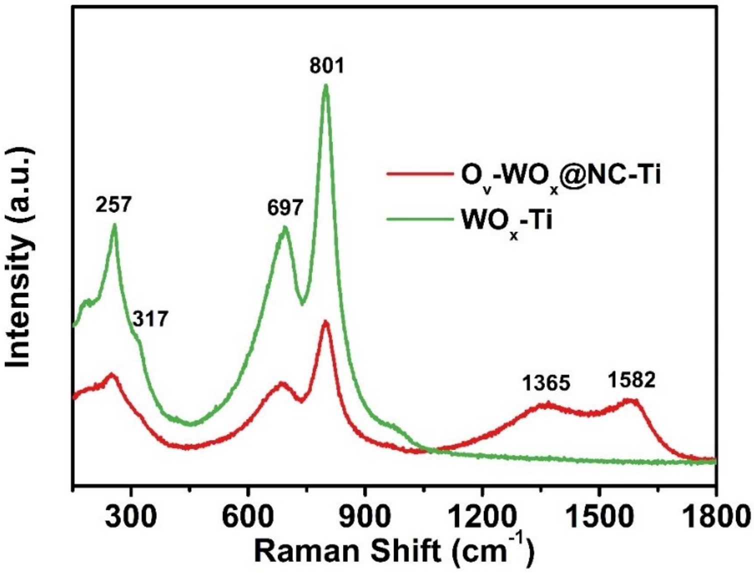


**Figure S5.** Raman pattern of $O_v$-$WO_x$@NC and $WO_x$ loaded on Ti foil.

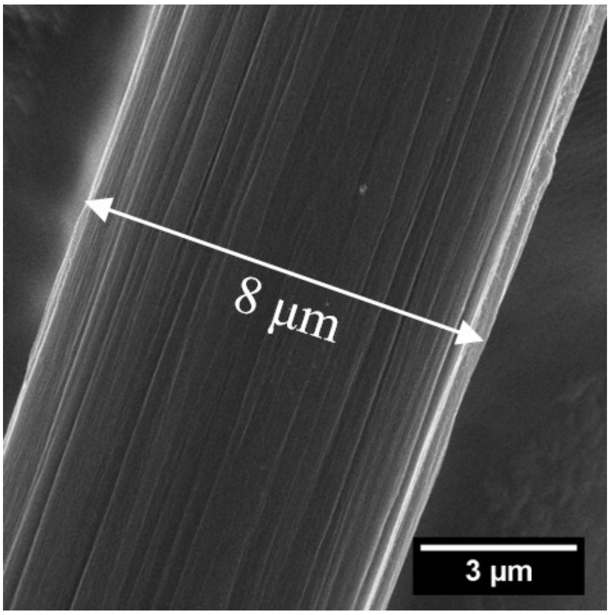

**Figure S6.** SEM image of the pristine CFP.

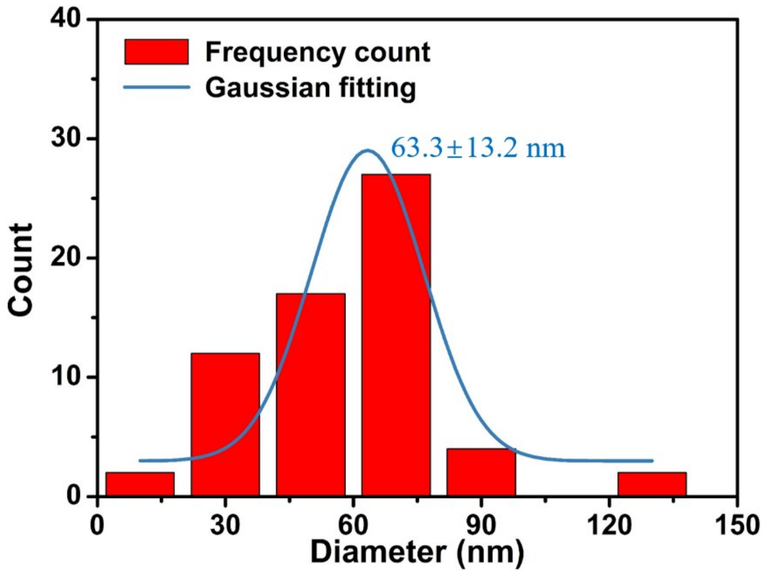


**Figure S7.** Diameter distribution of $O_v$-$WO_x$@NC. The dark cyan line shows the Gaussian fitting of data

**Table S1.** The amount of W, O, N, C and Ni in the composites detected by EDS analysis

| Catalysts | Atomic (%) | | | | |
|---|---|---|---|---|---|
| | W | N | C | O | Ni |
| $WO_x$ | 22.36 | -- | 33.06 | 44.59 | -- |
| $O_v$-$WO_x$@NC | 34.36 | 5.16 | 24.75 | 35.74 | -- |
| $O_v$-$WO_x$@NC-Ni | 30.01 | 4.51 | 22.94 | 37.06 | 5.49 |

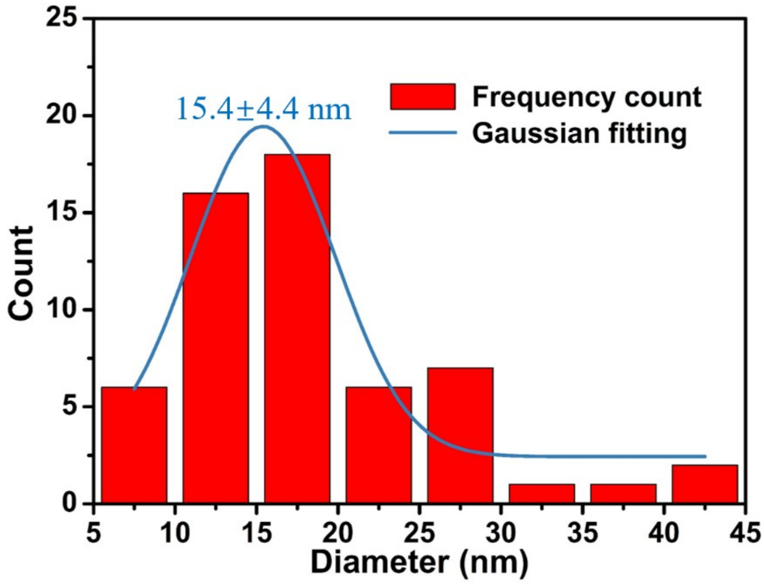


**Figure S8.** Diameter distribution of Ni nanoparticles. The dark cyan line shows the Gaussian fitting of data

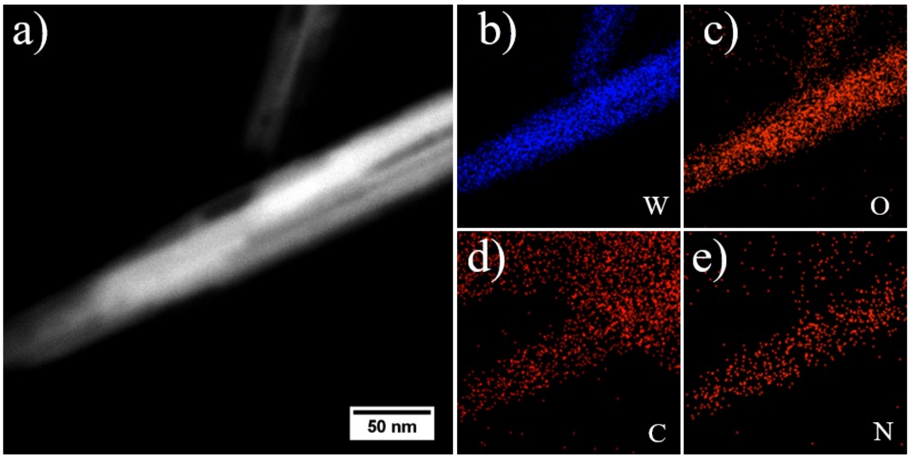


**Figure S9.** (a) Dark-field STEM image of $O_v$-$WO_x$@NC and corresponding elemental mapping images of (b) W, (c) O, (d) C and (e) N.

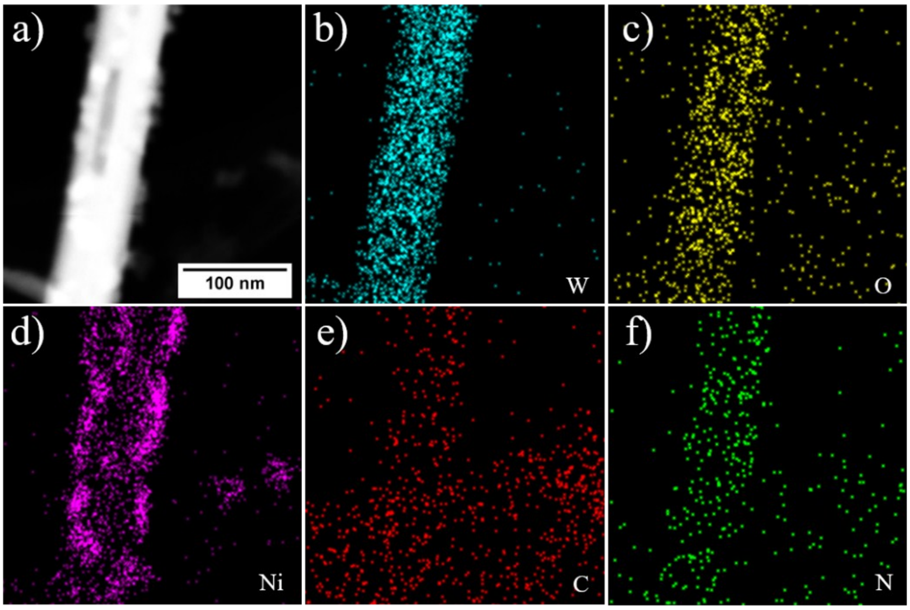


**Figure S10.** (a) Dark-field STEM image of $O_v$-$WO_x$@NC-Ni and corresponding elemental mapping images of (b) W, (c) O, (d) Ni, (e) C and (f) N.

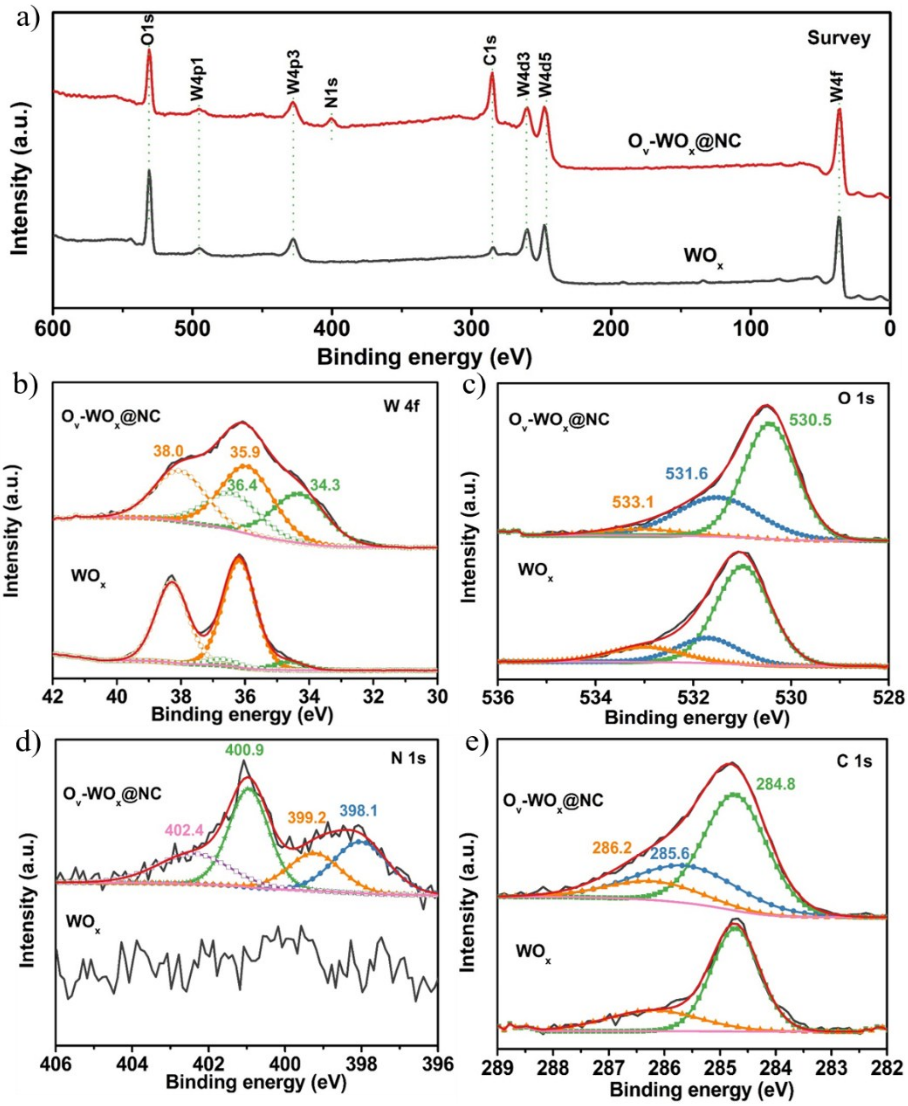


**Figure S11.** XPS spectra of $WO_x$ and $O_v$-$WO_x$@NC.

**Table S2.** The amount of W, O, N, C and Ni in the composites detected by XPS analysis

| Catalysts | Atomic (%) | | | | |
|---|---|---|---|---|---|
| | W | N | C | O | Ni |
| $WO_x$ | 15.32 | -- | 21.85 | 62.83 | -- |
| $O_v$-$WO_x$@NC | 9.02 | 8.79 | 58.2 | 23.99 | -- |
| $O_v$-$WO_x$@NC-2Months-Air | 7.66 | 9.5 | 58.91 | 23.93 | -- |
| $O_v$-$WO_x$@NC-5h-$H_2O_2$ | 11.61 | 7.53 | 38.72 | 42.14 | -- |
| $O_v$-$WO_x$@NC-Ni | 5.83 | 6.47 | 52.48 | 28.84 | 6.37 |
| $O_v$-$WO_x$@NC-Ni-it | 4.55 | 6.77 | 42.99 | 37.08 | 8.61 |

**Table S3.** Fitting parameters (peak position, peak area and species percentage) for both W $4f_{7/2}$ and W $4f_{7/2}$ spectra taken on the resultant samples.

| Samples | species | Peaks | | Area | | $W^{5+}/W^{6+}$ |
|---|---|---|---|---|---|---|
| | | $4f_{7/2}$ | $4f_{5/2}$ | $4f_{7/2}$ | $4f_{5/2}$ | |
| $WO_x$ | $W^{5+}$ | 34.6 | 36.7 | 4713 | 3535 | 1:13.82 |
| | $W^{6+}$ | 36.2 | 38.3 | 65119 | 48839 | |
| $O_v$-$WO_x$@NC | $W^{5+}$ | 34.3 | 36.4 | 13000 | 9750 | 1:1.31 |
| | $W^{6+}$ | 35.9 | 38.0 | 17242 | 12932 | |
| $O_v$-$WO_x$@NC-2Months-Air | $W^{5+}$ | 34.5 | 36.7 | 7522 | 5641 | 1:1.38 |
| | $W^{6+}$ | 35.4 | 37.5 | 10405 | 7804 | |
| $O_v$-$WO_x$@NC-5h-$H_2O_2$ | $W^{5+}$ | 34.7 | 36.9 | 11852 | 8889 | 1:1.43 |
| | $W^{6+}$ | 35.5 | 37.6 | 16999 | 12750 | |
| $O_v$-$WO_x$@NC-Ni | $W^{5+}$ | 34.2 | 36.3 | 9001 | 6750 | 1:1.26 |
| | $W^{6+}$ | 35.9 | 38.0 | 11295 | 8471 | |
| $O_v$-$WO_x$@NC-Ni-it | $W^{5+}$ | 34.8 | 36.9 | 5500 | 4125 | 1:1.55 |
| | $W^{6+}$ | 35.5 | 37.6 | 3540 | 2655 | |

**Table S4.** Fitting parameters (peak position, peak area and species percentage) for oxygen vacancies ($O_v$), W-O-W and O-C taken on the resultant samples.

| Samples | species | Peaks | Area | $O_v/O$ |
|---|---|---|---|---|
| $WO_x$ | $O_v$ | 531.7 | 22001 | 0.192 |
| | W-O-W | 530.9 | 76487 | |
| | O-C | 533.0 | 16002 | |
| $O_v$-$WO_x$@NC | $O_v$ | 531.6 | 12001 | 0.329 |
| | W-O-W | 530.5 | 22497 | |
| | O-C | 533.1 | 1999 | |
| $O_v$-$WO_x$@NC-2Months-Air | $O_v$ | 531.5 | 7675 | 0.338 |
| | W-O-W | 530.5 | 14501 | |
| | O-C | 533.1 | 499 | |
| $O_v$-$WO_x$@NC-5h-$H_2O_2$ | $O_v$ | 531.5 | 14121 | 0.327 |
| | W-O-W | 530.4 | 26941 | |
| | O-C | 533.1 | 2096 | |
| $O_v$-$WO_x$@NC-Ni | $O_v$ | 531.6 | 15770 | 0.334 |
| | W-O-W | 530.5 | 21001 | |
| | O-C | 533.2 | 8409 | |
| | O-Ni | 529.7 | 2001 | |
| $O_v$-$WO_x$@NC-Ni-it | $O_v$ | 531.7 | 12646 | 0.374 |
| | W-O-W | 530.7 | 15626 | |
| | O-C | 533.0 | 3532 | |
| | O-Ni | 529.8 | 1999 | |

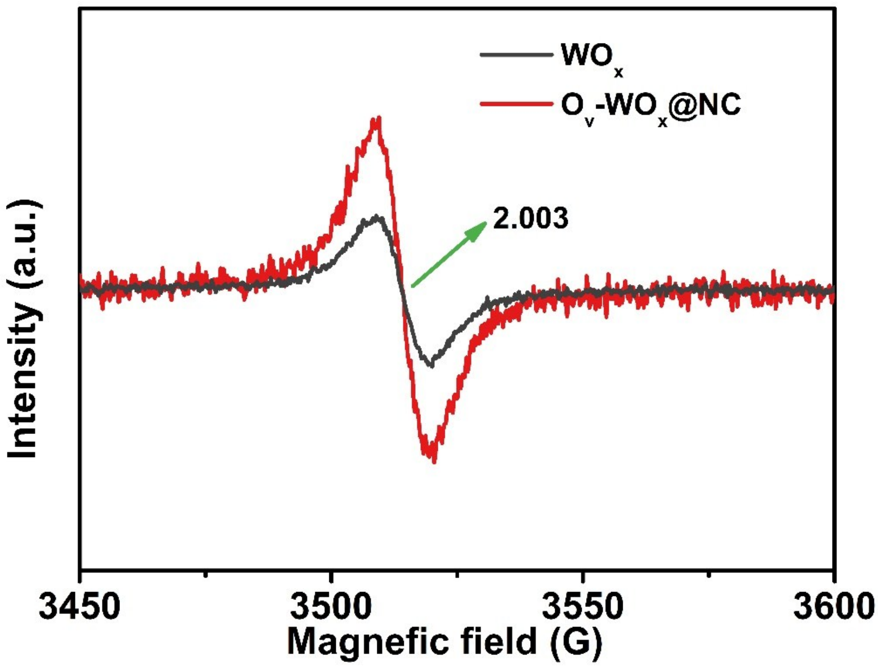


**Figure S12.** EPR spectra of $WO_x$ and $O_v$-$WO_x$@NC at room temperature.

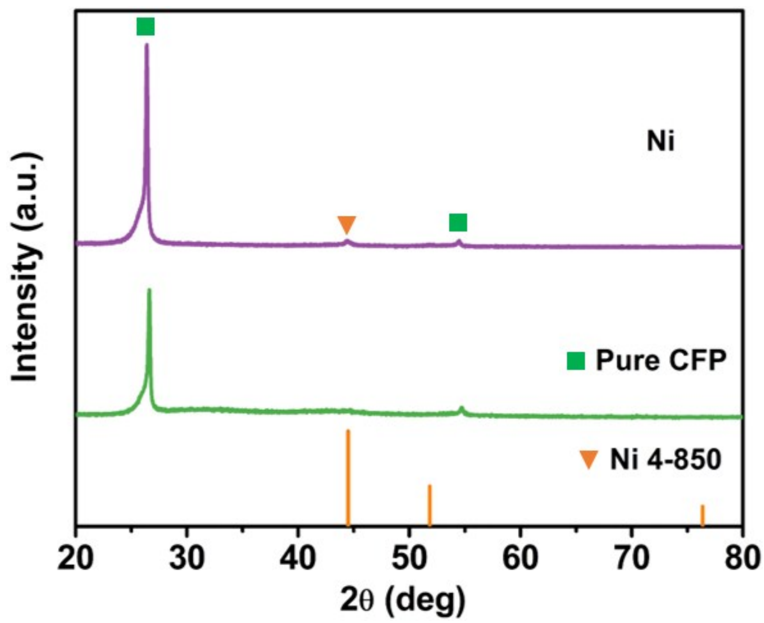

**Figure S13.** XRD pattern of Ni.

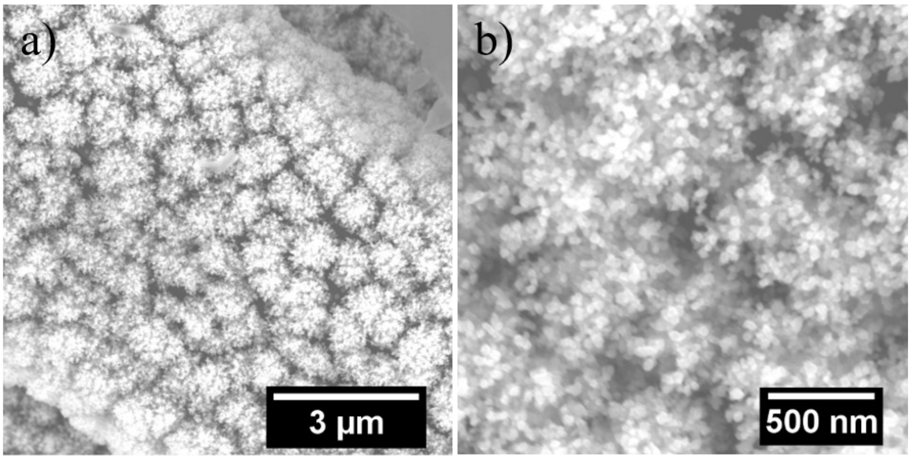

**Figure S14.** (a) Low- and (b) high-magnification SEM images of Ni.

**Table S5.** Performances of representative highly efficient TMOs-based HER catalysts in alkaline media.

| Reference | Catalyst | Mass density (mg cm$^{-2}$) | $\eta_{20}$ (mV) | $\eta_{100}$ (mV) | Tafel slope (mV/dec) | Counter electrode | Electrolyte |
|---|---|---|---|---|---|---|---|
| This work | $O_v$-$WO_x$@NC-Ni | 7.2 | 67 | 164 | 62 | Graphite rod | 1 M KOH |
| J. Mater. Chem. A, 2019, DOI: 10.1039/C9TA03652K | M-$Co_3O_4$ layer | 0.76 | 115 | 203 | 63 | Graphite rod | 1 M KOH |
| J. Mater. Chem. A, 2017, 5, 9655–9660 | $WO_2$ HN/NF | 1.57 | 75 | -- | 43 | Graphite plate | 1 M KOH |
| ACS Catal. 2018, 8, 5062-5069 | Co/$Co_2Mo_3O_8$ | 2.5 | 50 | 210 | 33 | Graphite rod | 1 M KOH |
| Inorg. Chem. Front., 2018,5, 3042-3045 | 3D $Ni_3N$-$CeO_2$ nanohybrid | -- | 105 | 200 | 122 | Graphite plate | 1 M KOH |
| Nano Energy, 2018, 43, 103–109 | NiO NRs-m-$O_v$ | 0.2 | 150 | 280 | 100 | Graphite rod | 1 M KOH |
| Nat. Commun,2015, 6, 7261 | Lithium-induced NiFeOx nanoparticles | 1.6 | 133 | -- | -- | Pt wire | 1 M KOH |
| Adv. Energy Mater. 2016, 6, 1600528 | mesoporous $MoO_{3-x}$ | 0.2 | 170 | -- | 56 | Graphite rod | 0.1 M KOH |
| Nanoscale, 2017, 9, 4409–4418 | NiO@NF | 3.5 | 420 | -- | 231 | Graphite rod | 1 M KOH |
| J. Am. Chem. Soc. 2015, 137, 2688-2694 | Cobalt-cobalt oxide/N-doped carbon hybrids | 0.42 | 280 | -- | 115 | Pt plate | 1 M KOH |
| Energy Environ. Sci., 2017, 10, 2563 | P-$Co_3O_4$ | 0.4 | 135 | 165 | 52 | Graphite rod -- | 1 M KOH |
| Angew. Chem. Int. Ed. 2017, 56, 1324-1328 | Hollow $Co_3O_4$ microtube arrays | -- | 190 | 290 | 98 | Pt wire | 1 M KOH |
| Inorg. Chem.2018, 57, 548-552 | $Ni_2P$-$CeO_2$/Ti mesh | 1.58 | 84 | 160 | 87 | Platinum wire | 1 M KOH |
| Nanoscale, 2018, 10, 2213-2217 | $CeO_2$-$Cu_3P$/NF | -- | 148 | 275 | 132 | Graphite sheet | 1 M KOH |

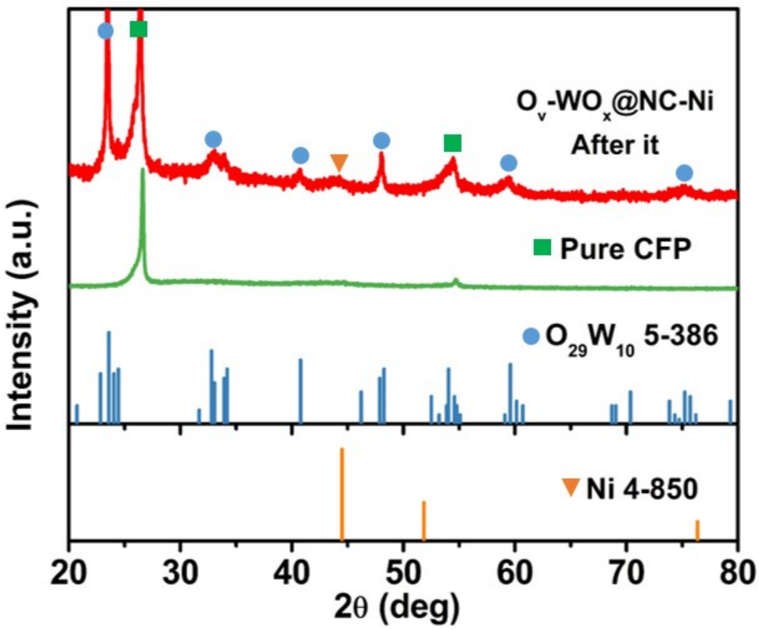


**Figure S15.** XRD pattern of $O_v$-$WO_x$@NC-Ni after the electrochemical measurement.

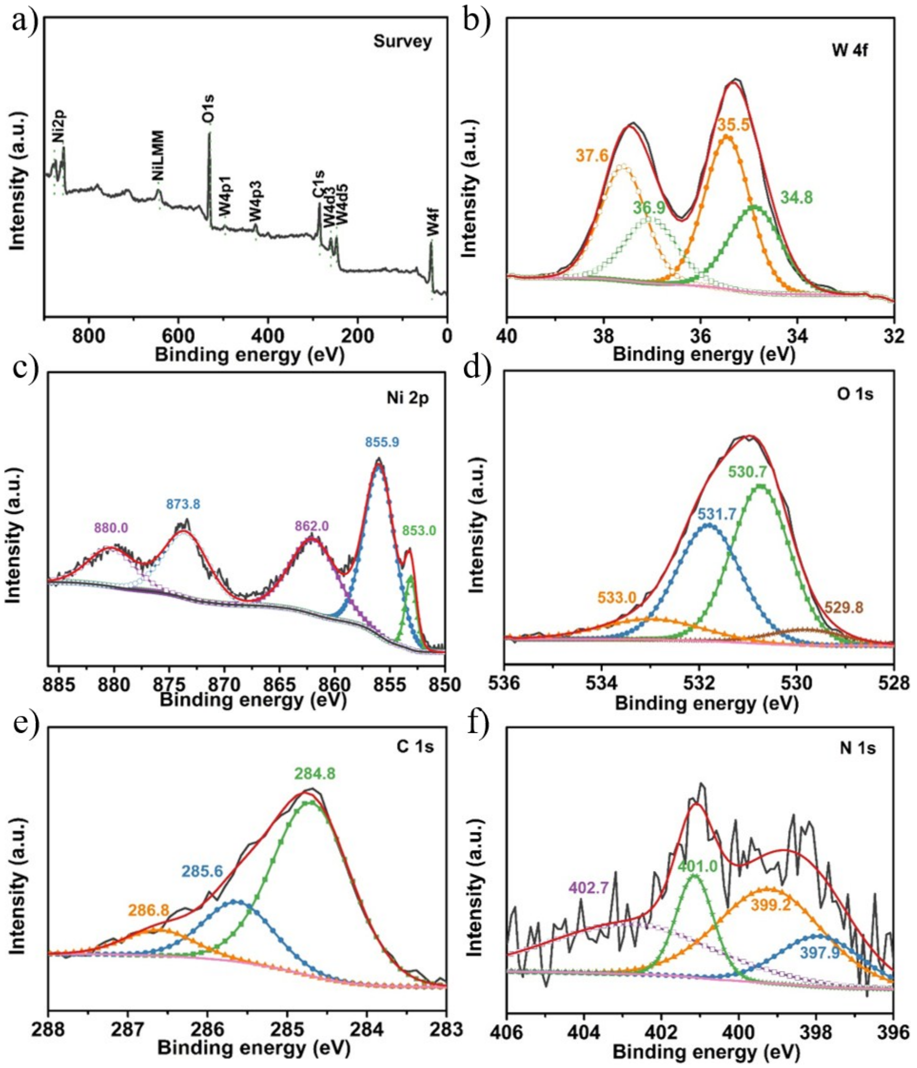


**Figure S16.** XPS pattern of $O_v$-$WO_x$@NC-Ni after the electrochemical measurement.

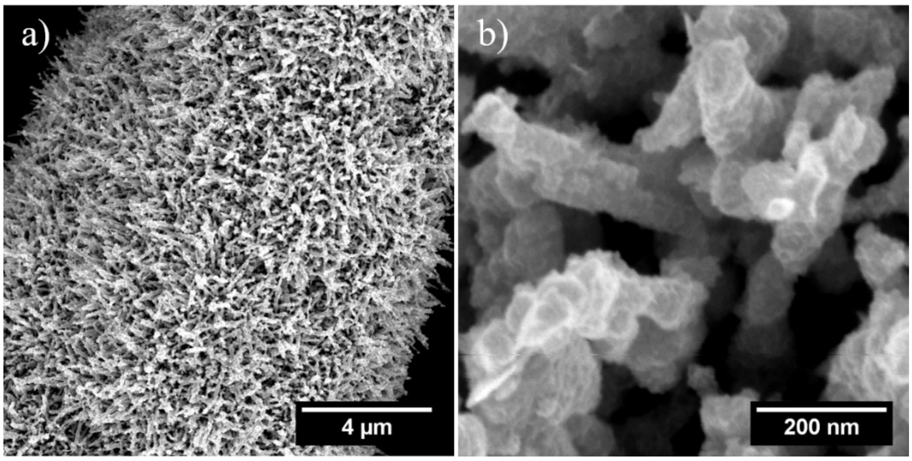


**Figure S17**. SEM pattern of $O_v$-$WO_x$@NC-Ni after the electrochemical measurement.

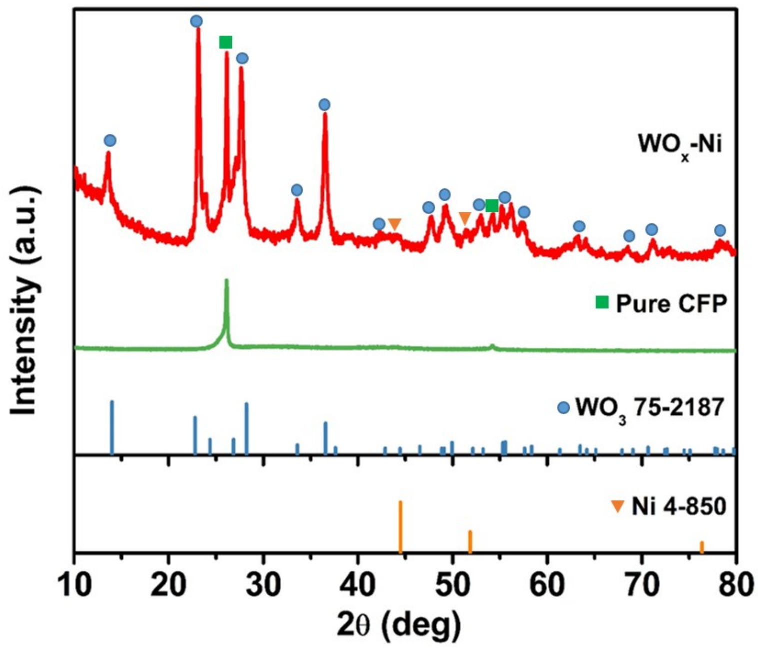


**Figure S18.** XRD pattern of $WO_x$-Ni.

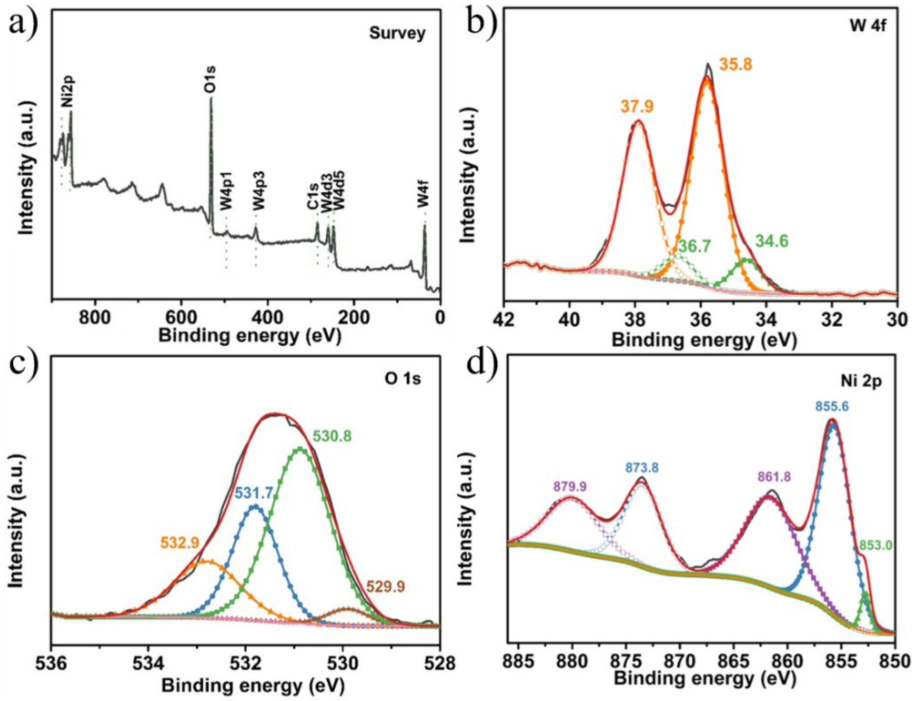


**Figure S19.** XPS pattern of $WO_x$-Ni.

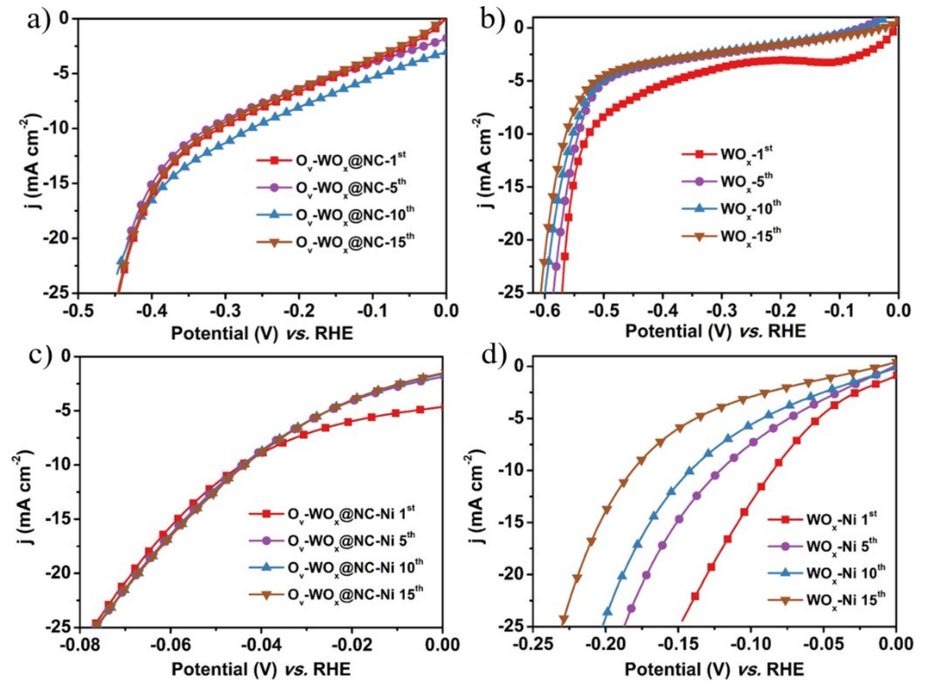


**Figure S20.** Polarization curves corresponding to different LSV activation scans of (a) $O_v$-$WO_x$@NC, (b) $WO_x$, (c) $O_v$-$WO_x$@NC-Ni and (d) $WO_x$-Ni.

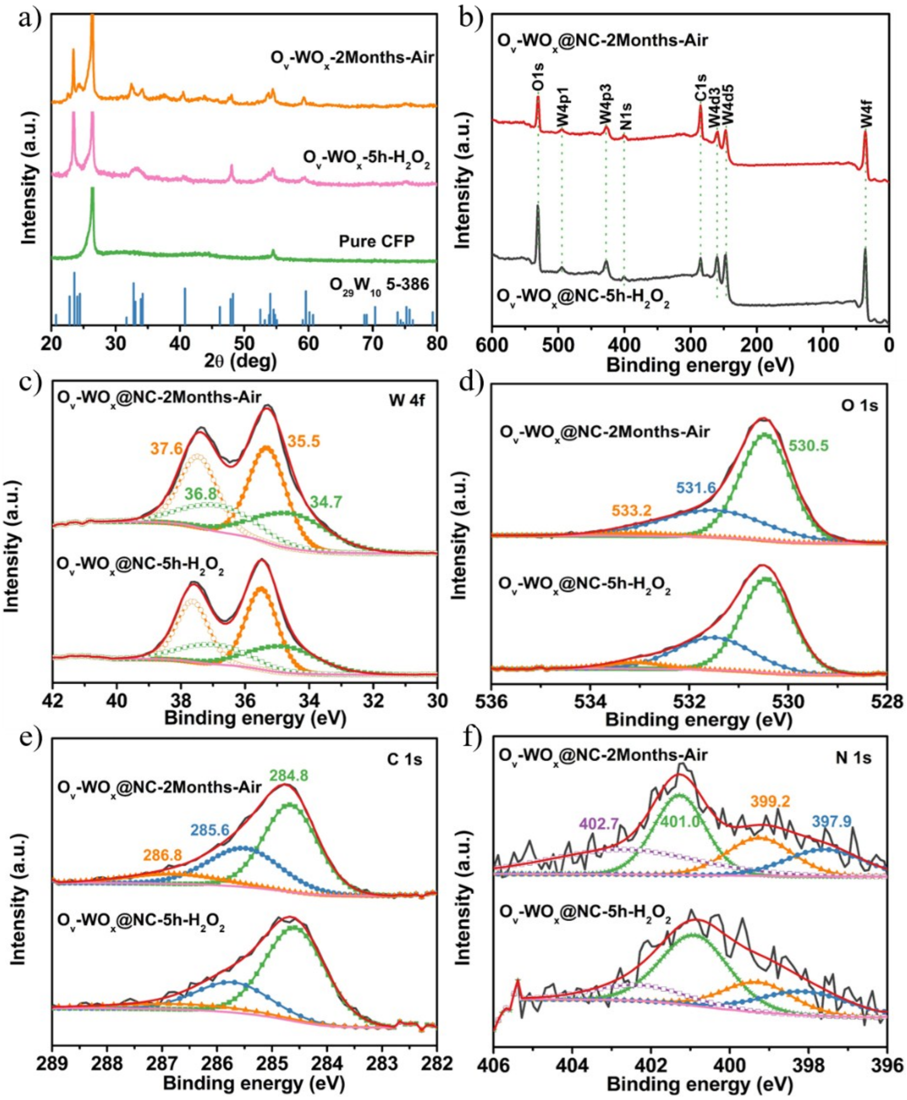


**Figure S21.** The XRD and XPS spectra of $O_v$-$WO_x$@NC-2Months-Air and $O_v$-$WO_x$@NC-5h-$H_2O_2$.

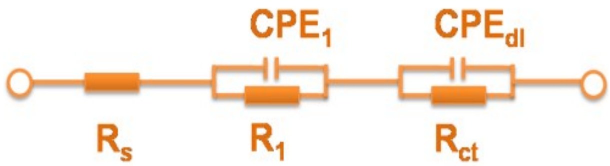


**Figure S22.** Equivalent circuit used to fit the EIS data. $R_s$ is the overall series resistance, $CPE_1$ and $R_1$ are the constant phase element and resistance describing electron transport at GCE/electrocatalyst interface, respectively, $CPE_{dl}$ is the constant phase element of the electrocatalyst/electrolyte interface, and $R_{ct}$ is the charge transfer resistance at electrocatalyst /electrolyte interface.

**Table S6.** The fitting results of EIS spectra in basic solution.

| Sample | $R_s$ (Ω) | $Q_1$ (F cm$^{-2}$ S$^{n-1}$) | $n_1$ | $R_1$ (Ω) | $Q_{ct}$ (F cm$^{-2}$ S$^{n-1}$) | $n_{ct}$ | $R_{ct}$ (Ω) |
|---|---|---|---|---|---|---|---|
| $WO_x$ | 1.958 | 1.605e-3 | 0.7521 | 2.041 | 0.04355 | 0.2032 | 570.2 |
| $O_v$-$WO_x$@NC | 1.062 | 1.199e-6 | 1 | 2.054 | 0.01373 | 0.7535 | 295.4 |
| Ni | 1.598 | 7.566e-6 | 0.8635 | 1.866 | 0.001688 | 0.7888 | 30.35 |
| $O_v$-$WO_x$@NC-Ni | 1.069 | 9.471e-7 | 0.9286 | 2.52 | 0.046 | 0.832 | 12.09 |

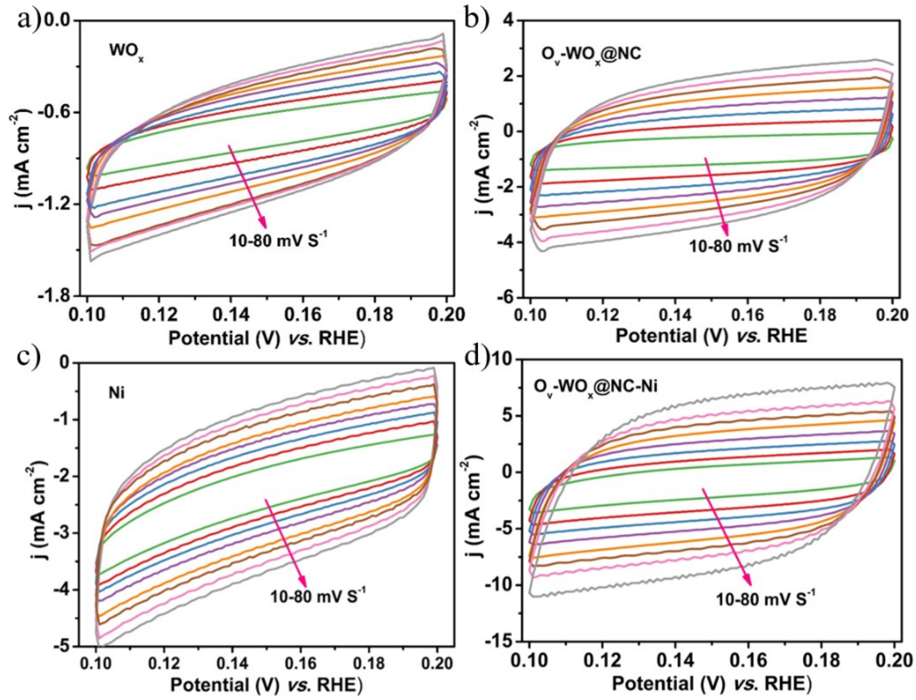


**Figure S23.** Cyclic voltammetry scans of (a) $WO_x$, (b) $O_v$-$WO_x$@NC, (c) Ni and (d) $O_v$-$WO_x$@NC-Ni.

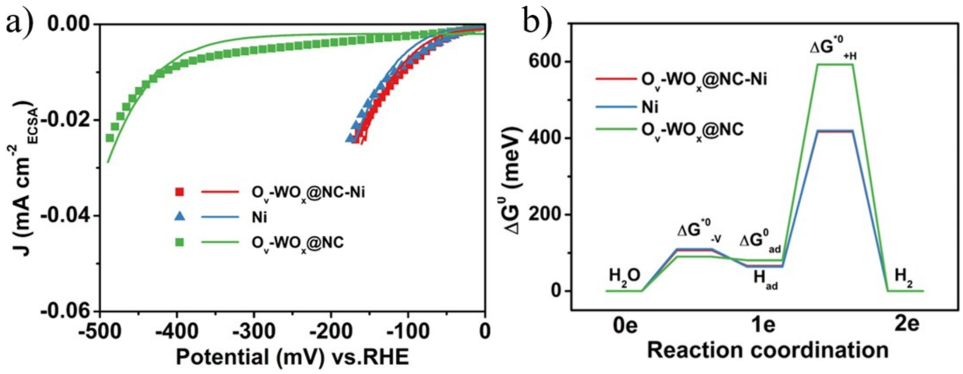


**Figure S24.** (a) Polarization curves normalized by ECSA: the scatters are experimental data, and lines are fitting curves using the dual-pathway kinetic model. (b) Free energy diagram in 1 M KOH fitted from $J_{ECSA}$.

**Table S7.** The fitting results of free energies corresponding to different steps during the HER.

| Sample | $\Delta G^{*0}_{-V}$ $(meV)$ | $\Delta G^{*0}_{+H}$ $(meV)$ | $\Delta G^{*0}_{+T}$ $(meV)$ | $\Delta G^{0}_{ad}$ $(meV)$ | $\Delta G^{*0}_{+H} - \Delta G^{0}_{ad}$ $(meV)$ |
|---|---|---|---|---|---|
| $O_v$-$WO_x$@NC | 90 | 593 | 962 | 81 | 512 |
| Ni | 110 | 420 | 1043 | 64 | 359 |
| $O_v$-$WO_x$@NC-Ni | 107 | 417 | 1041 | 66 | 351 |

$\Delta G^{*0}_{-V}$: the standard activation free energy for Volmer step.

$\Delta G^{*0}_{+H}$: the standard activation free energy for Heyrovsky step.

$\Delta G^{*0}_{+T}$: the standard activation free energy for Tafel step.

$\Delta G^{0}_{ad}$: the standard free energy of adsorption for the reaction intermediate.

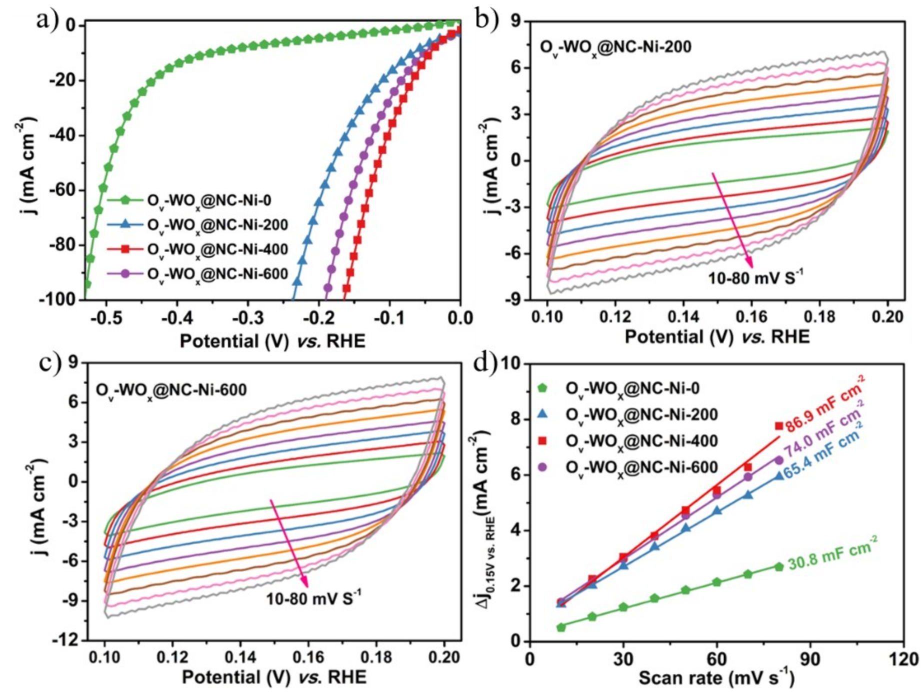


**Figure S25.** (a) Polarization curves of $O_v$-$WO_x$@NC-Ni-XX. XX is the electrodeposition time of Ni. $O_v$-$WO_x$@NC-Ni-0 is $O_v$-$WO_x$@NC mentioned above, and $O_v$-$WO_x$@NC-Ni-400 is also named as $O_v$-$WO_x$@NC-Ni. Cyclic voltammetry scans of (b) $O_v$-$WO_x$@NC-Ni-200 and (c) $O_v$-$WO_x$@NC-Ni-600. (d) Estimation of the $C_{dl}$ through plotting the current density difference ($\Delta J= 1/2(J_a-J_c)$ at 0.15 V vs. RHE obtained from the CV against scan rate to fit a linear regression.

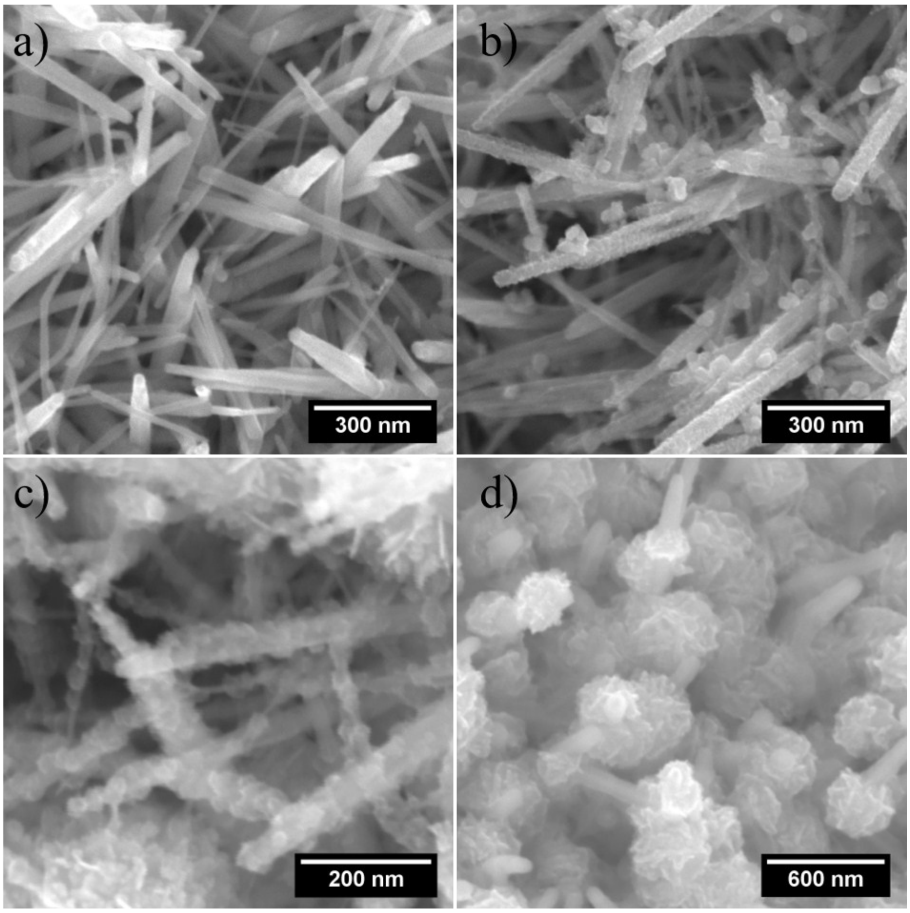


**Figure S26.** SEM iamges of (a) $O_v$-$WO_x$@NC-Ni-0 (i.e. $O_v$-$WO_x$@NC), (b) $O_v$-$WO_x$@NC-Ni-200, (c) $O_v$-$WO_x$@NC-Ni-400 (i.e. $O_v$-$WO_x$@NC-Ni) and (d) $O_v$-$WO_x$@NC-Ni-600.